



THESIS APPROVED BY

---

Date

---

[Michael Nichols], Ph.D.

---

[Hill], Ph.D.

---

[Wrubel], Ph.D.

---

Gail M. Jensen, Ph.D., Dean

DRAFT

TITLE:

SUBTITLE

---

by

DANIEL JUAREZ LUNA

---

A THESIS

Submitted to the faculty of the Graduate School of Creighton  
University in Partial Fulfillment of the Requirements for the degree of  
Master of Science in [Physics/Medical Physics] (choose one) in the  
Department of Physics

---

Omaha, NE

August 6, 2025

DRAFT

# **Abstract**

The abstract is a maximum 350 word, double-spaced summary of your work. The word count limit is important for upload to the Creighton Digital Repository.

This project can be found as a template on the Overleaf.com Latex-writing website.

# Acknowledgments

Thank your research team, advisor, committee, family and friends, etc. See previous theses for examples.

I would like to thank Kian for introducing me to Latex, Kyle and Bong for troubleshooting help, and Dr. Nichols for his help with thesis creation.

DRAFT

*For Dr. Nichols*

# Contents

<b>Abstract</b>	iii
<b>Acknowledgments</b>	iv
<b>Dedication</b>	v
<b>1 Introduction</b>	1
1.1 Literature review . . . . .	3
1.1.1 Magnetic Resonance Imaging (MRI): How it works? . . . . .	3
1.1.2 Safety . . . . .	4
1.1.3 Instruments? . . . . .	5
1.1.4 Previous studies summary . . . . .	5
1.2 Scope of Research . . . . .	5
<b>2 Materials and Methods</b>	9
2.0.1 Magnetic Field and Gradient Mapping Platform . . . . .	10
2.0.2 Translational Force Measurement via Angular Deflection . .	14
2.0.3 Torque Measurement Apparatus (In Progress) . . . . .	21
<b>A Engineering Drawings</b>	22
<b>B Calibrations</b>	25

C Copyright permissions	<b>29</b>
-------------------------	-----------

Glossary	<b>29</b>
----------	-----------

DRAFT

# List of Tables

DRAFT

# List of Figures

2.1	PVC-based magnetic field mapping platform used for spatial $B_0$ and $\nabla B_0$ measurement. As shown in Ferreira 2017 [1, 2]. . . . .	11
2.2	Flowchart of the Gaussmeter VI data acquisition algorithm. . . . .	13
2.3	Experimental pendulum-based apparatus constructed from PVC for MRI translational force measurements. . . . .	15
2.4	3D render of the design on lead holder . . . . .	16
2.5	Close-up of the epicardial lead fragment suspended by monofilament thread over the ruler. Image illustrates the displacement measurement system and the sample scale. . . . .	16
2.6	In-lab experimental setup for MRI translational force assessment. Labeled components include the solenoid, pendulum fixture, measurement tools, and control equipment. . . . .	18
2.7	Free-body diagram of device in magnetic field (adapted from ASTM F2052-15, Appendix X2). . . . .	20
2.8	Implementation of the apparatus in the laboratory setting. . . . .	21
B.1	Displacement as a function of current through the solenoid. . . . .	25
B.2	Measured angle $\alpha$ versus magnetic field intensity $B_0$ . . . . .	26
B.3	Computed translational force $F_m$ as a function of $B_0$ . . . . .	26
B.4	Residuals from linear fit of $\tan(\alpha)$ vs. $B_0 \cdot \frac{dB_0}{dz}$ . Error bars indicate propagated uncertainties. . . . .	27

B.5 Propagation of measurement uncertainty through magnetic field analysis. Top: Measured field  $B_0$  with standard deviation and SEM. Middle: Gradient  $dB/dz$  with propagated error. Bottom: Final product  $B_0 \cdot dB/dz$  with multiple uncertainty estimations (standard, fractional, SEM). This term was used as the independent variable in the susceptibility fit. . . . .

28

DRAFT

# Chapter 1

## Introduction

Medical diagnostics heavily rely on imaging tools such as MRI, a powerful and evolving application capable of showing high contrast sensitivity to soft tissue while not depending on ionizing radiation. However, safety concerns may arise during cardiac MRI procedures, electro cardigram (ECG) leads are generally cataloged as MRI unsafe because of the strong magnetic field and radiofrequency (RF) pulses that may interact with these leads.

Temporary epicardial pacing leads are frequently utilized as part of postoperative cardiac rhythm control procedures. When the surgical danger of removing these leads is too high, they are left in place to prevent further complications. These cases introduce long-term repercussions, most notably the loss of access to MRI. There is still a dearth of focused studies evaluating the precise dangers associated with retained epicardial leads, despite the frequent use of such leads and their repercussions. Existing clinical recommendations tend to be too cautious and frequently disqualify these individuals from MRI eligibility even when there is little evidence to support it.

In this document we will explain the current state of research on this matter, the main elements involved in the interaction of temporary epicardial leads and MRI - especially in relation to mechanical interactions like translational force and torque.

We will explore... and propose a methodology that tests these micro-Newton forces with precision

More than 300,000 individuals are receiving new cardiac implantable electronic device (CIED) implants every year in the U.S. alone, reported the Heart Rhythm Society (HRS) in 2024 [3]. Some of these patients will eventually require device explantation or revision, necessitating surgery [4]. For this, there is a protocol to monitor cardiac rhythm that involves the use of temporary epicardial leads, however there is a recognized practice when these leads are removed -only if significant resistance is encountered- to cut the wire flush with the skin, intentionally leaving a small segment inside the patient to prevent immediate complications [5, 6, 7].

These provisional leads are frequently placed during open-heart surgery to regulate cardiac rhythm postoperatively, then are typically cut at the skin surface leaving behind a short length of wire embedded in the tissue [8]. In general, a device labeled as MRI safe is expected to be nonconductive, non-electrical, non-magnetic, and to present no known hazards in the MRI environment. However, this classification does not apply to most epicardial leads, as they are rarely physically characterized after removal. By the time they are cut, these leads have fulfilled their clinical purpose, and systematic safety evaluations are seldom performed. Although retained leads are nonfunctional and relatively short, they are frequently classified as MRI unsafe due to concerns over RF heating, magnetically induced translational forces and torques, or inadvertent cardiac stimulation [9, 10, 11]. Effectively preventing patients with CIED or cardiac surgery history, who are most likely to need a MRI scan during their lifetime, to not be able to enter MRI room.

Recent studies regarding this problem have shown both no image quality degradation and, most importantly, no serious safety events such as, device malfunction, myocardial injury or arrhythmias, associated with MRI examinations in patients with CIEDs abandoned leads, including epicardial leads [12, 13]. While these work have

evaluated to some extent the resulting consequences of RF-induced heating, mechanical forces and conductivity, detail is needed. For example translational motion and torque remain physically under-characterized.

In that regard, the primary safety concerns regarding retained cardiac leads during MRI arise from three main interaction mechanisms. First, the strong magnetic field and its spatial gradient can exert translational forces and torques on the lead, resulting in mechanical displacement. Second, the lead can absorb energy from the MRI's (RF) field, potentially causing localized heating that poses a thermal risk to the patient. Third, the RF field may induce alternating currents within the lead, which can electrically stimulate nearby cardiac tissue, potentially leading to dangerous physiological effects.

To properly situate this work, the following section will review pertinent literature on MRI devices, MRI safety principles, electromagnetic theory, lead design, lead-MRI interactions and previous studies to establish the technical and clinical context needed to fully understand the motivations and significance of this study.

## 1.1 Literature review

### 1.1.1 MRI: How it works?

MRI or Magnetic Resonance Imaging is a medical imaging modality that uses magnetic fields and radiofrequency (RF) energy to produce images, rather than ionizing radiation like X-rays making it inherent safe. MRI machines are capable of archiving high contrast sensitivity to soft tissue differences because of the reliance on micromagnetic properties of the tissue and its inherent differences leveraging on Proton Density (PD) and the relaxation phenomena.

forces are described as a function of the static field strength ( $B_0$ ), its spatial gradient ( $\nabla B_0$ ), and the magnetic susceptibility ( $\chi$ ) and density ( $\rho$ ) of the material. A

well known and expected behavior is the magnetic pull on high susceptibility materials toward regions of higher field strength, like near the bore entrance of the scanner where the spatial gradient is highest [5, 14, 15]. For instance, a nonmagnetic stainless steel wire with  $\chi \approx 103$  ppm may experience a force equivalent to  $\sim 30\%$  of its weight, whereas ferromagnetic materials like pure nickel can experience forces exceeding 20,000 times their own weight. That is more than enough to become dangerous projectiles unless restrained [5, 15].

### **Components:**

For heat and electricity we are particularly interested on RF fields for mechanical we need to know the static magnetic field the mechanism and intensity of the field

Now we can explain the interactions between the two. Once RF is understood we can explain how this affects the leads resulting in heating and electric conductivity, based on the past local research and literature.

the physics

Resonance and Signal Generation

Tissue Contrast (Relaxation Phenomena)

the interaction

### **1.1.2 Safety**

the safety the 5 gauss line the examples of safety ASTM translational and torques studies the current protocols to assess objects near MRI field how this is different for us, size and susceptibility

ASTM F2052-21 offers a standardized technique for assessing magnetically induced displacement force on medical equipment in order to set safety standards for such situations. This standard states that a device is MR Conditional if the deflection

force it encounters in the MRI environment is less than the force of gravity upon it. This is usually verified if the deflection angle from vertical is less than  $45^\circ$  [16, 17].

### 1.1.3 Instruments?

Gaussmeter and Hall effect?

### 1.1.4 Previous studies summary

Previous studies made in our institution seek to illustrate the interaction of leads with the RF field in terms of energy absorbed and heat produced. It showed that lead length, type, and orientation significantly influence heating behavior. This study found that short leads ( $< 13$  cm) posed no significant thermal hazard during MRI at a specific absorption rate (SAR) of 2 W/kg and is thoroughly described as Master Thesis in 2021 [1, 18, 5].

Along the same line of thought, we aim to cover the mechanical aspect of lead-MRI interaction covering (1) Characterization of the static magnetic field, (2) quantification of translational forces near the bore entrance, (3) Torque evaluation from bore entrance to isocenter.

While some preliminary work has been conducted in our lab on these mechanical concerns, it remains unpublished, making this thesis a critical step in formalizing and extending that foundational effort.

## 1.2 Scope of Research

From here onwards I only stated the answers to some common questions the intro addresses.

What is the nature and scope of the problem you investigated?.

This research addresses the safety implications of retained temporary epicardial pacing leads during MRI procedures. Although these leads are commonly left in place after cardiac surgeries to avoid surgical risks, their presence is often treated as a contraindication for MRI access due to theoretical concerns over RF-induced heating, induced currents, and mechanical forces. While some studies have begun to evaluate heating and image quality, the mechanical interactions—specifically translational forces and torque—remain undercharacterized. This thesis focuses on quantifying those mechanical forces in order to clarify whether the static magnetic field in MRI poses a real risk to patients with retained leads.

What is the clear objective of your research?.

The primary objective of this study is to experimentally characterize the translational magnetic forces acting on retained epicardial pacing leads near the MRI bore entrance, and to map how those forces evolve with distance from the isocenter. This aims to directly assess whether the magnitude of such forces constitutes a meaningful mechanical risk in clinical settings.

What's the specific hypotheses or research questions that your study addressed?.

The central research question is: Do retained epicardial pacing leads experience translational magnetic forces within an MRI environment that are clinically significant enough to justify current safety restrictions?

What is your purpose in writing this paper?

The purpose of this thesis is to provide experimental evidence on MRI-induced mechanical forces acting on retained cardiac leads, with the goal of informing clinical decision-making regarding MRI safety. By addressing a gap in the literature, the study seeks to support more nuanced guidelines that balance patient safety with access to essential imaging.

What method of investigation did you use in your study?.

In the lab, the investigation used a PVC controlled pendulum-based measurement setup simulating exposure to a magnetic field gradient similar to that found at the MRI bore entrance. A solenoid coil was employed to replicate the spatial gradient of the static magnetic field, and micro-Newton displacements were recorded to estimate translational forces on test rods. For torque a set of neodymium magnets would create the static field while a metallic rod would be fixed in a position perpendicular to the field with an attachment and be allowed to rotate, counter forces would then be measured out the attachment with a circuit and sensor of our own fabrication.

What were the reasons for choosing your particular method?.

These methods allow for high sensitivity in detecting small magnetic forces in a controlled environment, without the complications of patient variability or direct MRI scanner use. The pendulum approach provides a clear physical model that isolates translational force components for precise characterization. The torque model allows to independently assess strength of force exerted.

Materials and methods bridge [placeholder]

What are the few key concepts and themes that will run through all parts of your thesis, starting from this introduction?

The thesis will consistently engage with 1 of the 3 main interaction modes between MRI and retained leads: mechanical forces, RF-induced heating, and induced currents. In these mechanical forces aspect we particularly care about translational and rotational displacement due to static field gradients. Concepts from electromagnetism, MRI safety standards, and biomedical device regulation form the thematic backbone of the work.

Measurements are interpreted in the context of magnetic susceptibility theory and compared to relevant thresholds from the literature [1, 17]. These techniques will help with more thorough evaluations of MRI safety in patients with retained temporary epicardial leads and set the stage for a future clinical adaptation of the protocol

employing a 1.5 T MRI scanner. This method aids in the improvement of device classification and the creation of uniform experimental procedures for the assessment of torque and translational safety.

DRAFT

# Chapter 2

## Materials and Methods

The objective of this study was to measure and quantify MRI-induce translational and torque forces experienced by an post-surgical epicardial pacing leads when exposed to the static magnetic field. Safety limits for MRI magnetic fields are well established and described in the Introduction, based on ASTM F-series guidelines. Following these methods, we constructed non-magnetic test apparatus specifically designed to measure these forces with the precision required for clinical applications.

However, clinical access for experimental testing posed a significant challenge, as MRI scanner time is typically associated with long scheduling delays and short available measurement periods. Therefore, a secondary objective of this work was to improve the quality of our experimental setup in order to maximize the efficiency of data acquisition during these limited observation windows.

Previous students developed the laboratory-scale instruments and associated software necessary to evaluate magnetic forces in a controlled environment. This was achieved by generating a smaller but reproducible magnetic field in the laboratory, enabling characterization of materials with relatively high magnetic susceptibility. While this laboratory-generated field was not sufficient to directly measure or characterize the epicardial lead itself, it allowed for evaluation of the accuracy and mea-

surement capacity of each instrument, as well as for the observation of the physical phenomena described above. Furthermore, given the proportional nature of the magnetic effects on a material, it was expected that, when tested in the much stronger (3 T) magnetic field of a clinical MRI system, the small magnetic susceptibility of the epicardial lead would not present a significant limitation in terms of measurement accuracy.

Three distinct experimental setups were involved in this study: (1) a spatial field mapping platform to characterize  $B_0$  and  $\nabla B_0$ , (2) a pendulum-based deflection apparatus to assess translational force through angular displacement, and (3) a torque measurement system for rotational force assessments. In this chapter we will explain our setup and rationale, as well as the proven modifications to the instruments in order to provide a reproducible map of action to test our instruments.

## Magnetic Field Generation

Magnetic fields were generated using a **custom-built air-core solenoid**, approximately 15 cm in length and 10 cm in outer diameter. The solenoid was densely wound with **copper wire (~1 mm diameter)**, forming an inner core of approximately 5 cm. A **Pasco Scientific SF-9584 DC power supply** was used to deliver currents in the range of **0–4 A**, corresponding to magnetic field strengths from **1 to 18.9 Gauss** for this solenoid. The system operated in a continuous mode; no rest periods were applied between trials due to the time required to stabilize the pendulum after each adjustment.

### 2.0.1 Magnetic Field and Gradient Mapping Platform

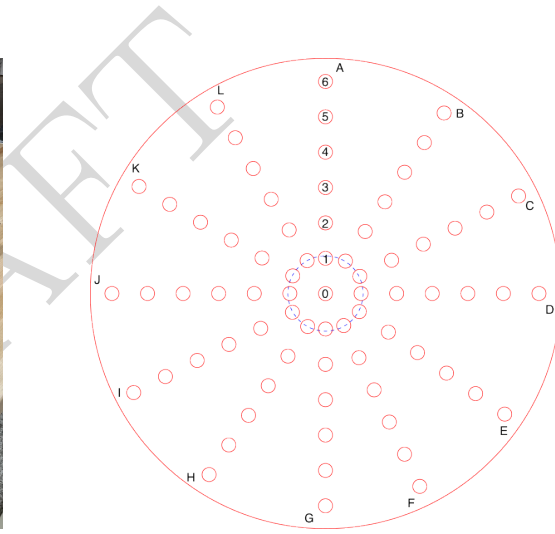
Magnetic field strength ( $B_0$ ) and gradient ( $\nabla B_0$ ) measurements were performed using a commercial Gaussmeter (Model GM2, AlphaLab Inc., Salt Lake City, UT). The GM2 operates on the Hall effect principle, wherein a voltage is generated across

a probe when exposed to a perpendicular magnetic field. This voltage is proportional to the local magnetic flux density, enabling precise spot measurements of field magnitude. The Gaussmeter used has an accuracy of 1% of the DC reading in the 16°C to 29°C range.

To ensure spatial accuracy and reproducibility, a fixture made from rigid Polyvinyl Chloride (PVC) was constructed by previous Creighton University students [1]. The platform comprises a 300 mm square base and a 280 mm diameter vertical circular plate, perforated with a 5x5 grid of probe-access holes spaced at 20 mm intervals as shown in figure 2.1. Each access point was numerically indexed to facilitate 2D field mapping in the X-Y plane.



(a) PVC-based mapping platform.



(b) Example field map output from MRI fringe region.

Figure 2.1: PVC-based magnetic field mapping platform used for spatial  $B_0$  and  $\nabla B_0$  measurement. As shown in Ferreira 2017 [1, 2].

Once the field-mapping phantom and Gaussmeter probe are co-aligned, data capture was streamlined to be sufficiently flexible and precise for our proximity measurements near an MRI. The manufacturer's default software, AlphaApp, provides basic data-logging, tethered or standalone recording, live screen streaming, and plotting of measurements from USB-enabled AlphaLab meters[19]. However, AlphaApp \*\*does not expose control over sampling frequency or allow real-time adjustment of acquisi-

tion parameters\*\*, limiting fine-grained temporal resolution when the probe is moved into steep field gradients. In contrast, using LabVIEW Virtual Instrument (VI) (VI) interface allows for configurable sampling intervals, buffer control, and precise timing protocols, enabling us to push the device for much higher accuracy as the probe approaches and crosses isocontour regions within the MRI fringe. We developed that VI by leveraging the AlphaLab Data Acquisition Communication Protocol to command the device directly via USB, providing deterministic control over timing and sample rate [20].

The data acquisition procedure for magnetic flux mapping is organized in this VI, whose basic logic is summarized in Figure 2.2. Upon startup, the VI initializes serial communication with the Gaussmeter, loads user-defined parameters (such as file name, mode of acquisition, delay time, and probe coordinates), and clears buffers in preparation for logging. The user may select either a continuous or an individual sampling mode. In continuous mode, the VI iterates through a defined number of data points with a fixed delay between samples; in individual mode, each data capture is triggered manually, allowing for precise positioning or timing. For both modes, each cycle involves reading the spatial coordinates, sending a measurement command, recording the returned magnetic flux value, and updating a graphical display as well as the output file.

While the flowchart reflects the core logic, it does not fully convey the customization added to the VI interface. For example, the front panel includes input fields for patient table (couch) parameters such as couch speed and displacement points. As mentioned above, our phantom is discretized with radial and angular indices: angular positions span 12 sectors clockwise from the 12 o'clock position (0 to 11 or A to L), and radial depths range from the center (0) to the outer edge (6). The probe's spatial location is represented in polar coordinates, and the system plots magnetic flux as a

function of position rather than time, allowing for intuitive visualization of the MRI fringe field across the phantom surface.

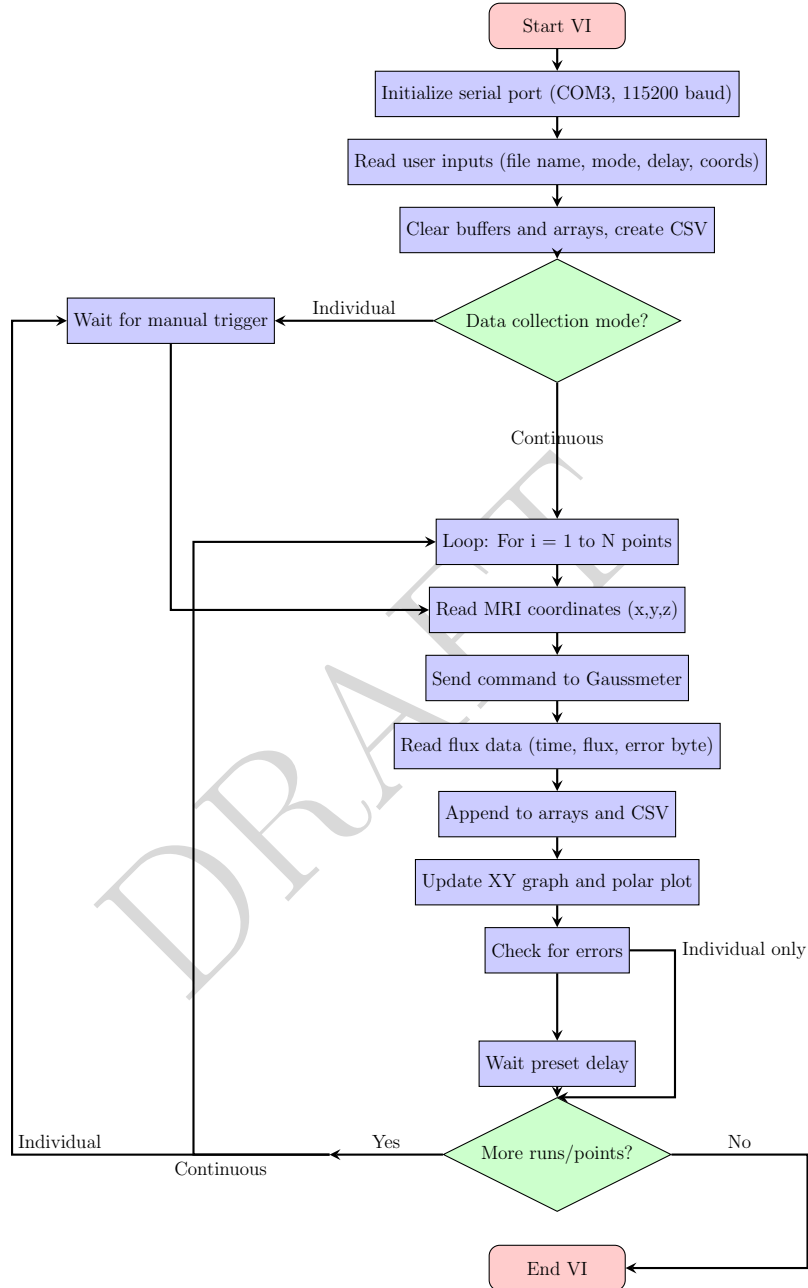


Figure 2.2: Flowchart of the Gaussmeter VI data acquisition algorithm.

In clinical use, the entire fixture is intended to be shifted axially along the Z-direction of a horizontal bore MRI scanner using controlled couch increments (e.g., 10 cm). This translation allows for volumetric sampling of  $B_0$  over several planes.

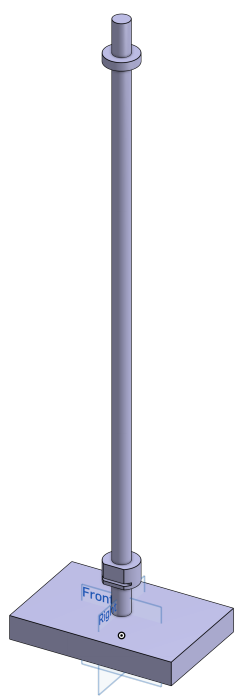
The spatial magnetic field gradient  $\nabla B_0$  can then be estimated numerically using finite difference calculations between adjacent measurement points. This method has previously been applied to MRI mapping in the work by Ferreira [2].

## 2.0.2 Translational Force Measurement via Angular Deflection

### Measurement Device

To assess MRI-induced translational forces in a laboratory environment, Creighton University developed a pendulum-style apparatus following the geometry and physics outlined in ASTM F2052-15[17]. The vertical post includes a screw clamp mechanism that enables height adjustment; however, a default suspension height of 1 meter was used for consistency across trials.

The experimental frame was constructed entirely from PVC components (Figure 2.3a), including a vertical post of 1.5 meters and a rigid base for stabilization. The sample—a **solid ferromagnetic cylinder** (length = 6 mm, diameter = 3 mm, mass = 0.3648 g, density = 8.6 g/cm<sup>3</sup>)—was suspended by a **955 mm-long sewing thread**, tied via a simple knot at its center. For clinical applications, a **0.25 mm nylon monofilament** is recommended for improved reproducibility and safety. A Monofilament Nylon thread has low stretch, complies with MR-safe properties (Non-metallic, Non-conductive, Non-magnetic), and reduces variability introduced by torsional drift or thread elasticity [16, 17]. The bottom of the sample was free to swing, forming a pendulum under gravity. A horizontal ruler, fixed along the Z-axis, served as the visual reference to quantify lateral displacements as shown in Figure 2.3b and detailed in Figure 2.5.



(a) CAD render of the pendulum apparatus created using CATIA.



(b) Real-life implementation of the apparatus in the laboratory setting.

Figure 2.3: Experimental pendulum-based apparatus constructed from PVC for MRI translational force measurements.

### Lead Holder Frame Design

To accommodate epicardial lead positioning while maintaining MRI compatibility, we propose the use of a lightweight, non-magnetic bee comb mesh also fabricated from Polylactic Acid (PLA). The suggested mesh dimensions are 16 mm length by 14 mm wide, with a thickness of 1 mm, for a total volume of less than  $100mm^3$  equivalent to around a tenth of 1 gram given the 1.24 grams per cubic centimeter ( $g/cm^3$ ) PLA density.

As shown in figure 2.4 and 2.5.

The mesh needs to be suspended such that the lead axis was aligned approximately parallel to the magnetic field gradient (Z-axis). The mesh's lightweight design aimed

to minimize its contribution to the total magnetic force, however its mass was not explicitly subtracted from the translational force calculations.

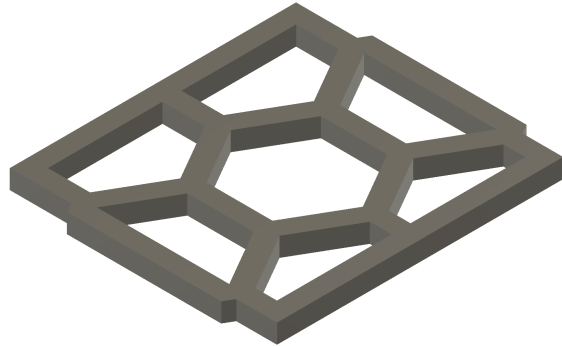


Figure 2.4: The design on lead holder comprises a rectangular lightweight bee comb mesh to wrap the epicardial lead around and hold it in a pendulum with a nylon string

A summary schematic of the apparatus and frame are included in Figures 2.3 and 2.4, with additional engineering drawings available in

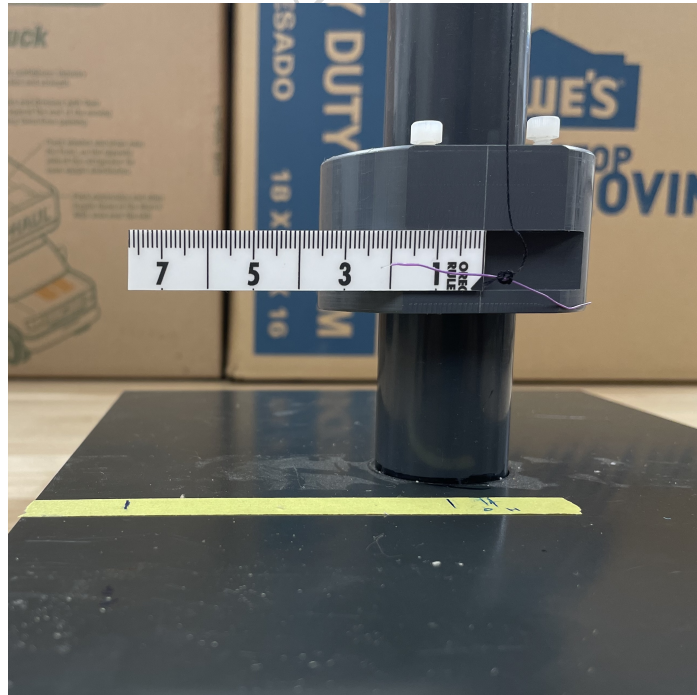


Figure 2.5: Close-up of the epicardial lead fragment suspended by monofilament thread over the ruler. Image illustrates the displacement measurement system and the sample scale.

## In Lab Measurement Protocol

Magnetic field measurements were performed using the **AlphaLab Inc. Gaussmeter** described before. The setup consisted of a custom-made solenoid connected to a Pasco power supply capable to deliver up 8 A acting as variable magnetic field generator for our experiment, the subject - a small ferromagnetic rod - was attached to a string pending from the MRI safe pole and angle of deflection was measured visually with a ruler on the subject horizontal displacement towards the coil. The Gaussmeter was positioned such that it allowed for small displacements and magnetic field measurements at the same time as angle deflection.

Figure 2.6 shows the experimental lab setup used to assess the methodology accuracy and reliability with all used components.



1. Power Supply with Ammeter  $\pm .001$  A
2. Solenoid (1 to 20 Gauss)
3. Ruler (Deflection Angle)  $\pm 1$  mm
4. PVC String Pole
5. Ferromagnetic Cylinder
6. AlphaLab, Inc. Gaussmeter  $\pm 0.001$  G

Figure 2.6: In-lab experimental setup for MRI translational force assessment. Labeled components include the solenoid, pendulum fixture, measurement tools, and control equipment.

To characterize local field gradients, measurements were taken at three positions: at the pendulum's equilibrium position, 0.5 mm below, and 0.5 mm above, yielding values of  $B_{-0.5}$ ,  $B_0$ , and  $B_{+0.5}$ , respectively. Each position was sampled **nine times per current level**, and gradients were computed using python pandas library and the central finite difference method:

$$\frac{dB}{dz} \approx \frac{B_{+0.5} - B_{-0.5}}{1 \text{ mm}} \quad (2.1)$$

Once the pendulum reached equilibrium under each magnetic condition, the horizontal displacement on  $z$  was recorded visually using the ruler as a reference. With known suspension length  $L$ , the **deflection angle**  $\alpha$  was calculated as:

$$\alpha = \tan^{-1} \left( \frac{x}{L} \right) \quad (2.2)$$

Following ASTM F2052-15, the translational force exerted on a device due to a static magnetic field spatial gradient can be evaluated through angular deflection. In this setup, the test object is suspended in equilibrium, and the balance of forces leads to:

$$\tan \alpha = \frac{F_m}{mg} \quad (2.3)$$

where  $\alpha$  is the deflection angle from vertical,  $F_m$  is the magnetically induced translational force,  $m$  is the mass of the object, and  $g$  is the gravitational acceleration. Rearranging gives:

$$F_m = mg \tan \alpha \quad (2.4)$$

This is also derived from Newtonian force balancing as in Appendix X2 of ASTM F2052-15 (Fig 2.7), and is valid even in cases when the magnetic force does not operate exactly at the center of mass. As a result, the approach is reliable for evaluating a variety of devices.

For materials where magnetization is induced by a static field (e.g., paramagnetic or unsaturated ferromagnetic materials), the translational force can also be expressed in terms of volumetric magnetic susceptibility  $\chi$ , assuming linear response:

$$F_m = \frac{\chi V}{\mu_0} B_0 \frac{dB_0}{dz} \Rightarrow \chi = \frac{\mu_0 F_m}{V B_0 \frac{dB_0}{dz}} \quad (2.5)$$

Combining this with the earlier result:

$$\chi = \frac{\mu_0 mg \tan \alpha}{V B_0 \frac{dB_0}{dz}} \quad (2.6)$$

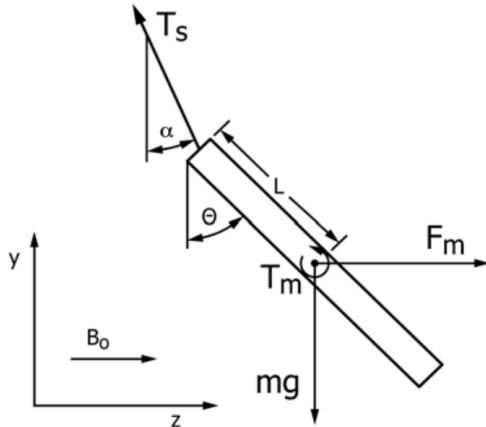


**FIG. X2.1 Free Body Diagram of Device in Magnetic Field**

Figure 2.7: Free-body diagram of device in magnetic field (adapted from ASTM F2052-15, Appendix X2).

This provides a direct estimation of magnetic susceptibility from angular deflection measurements, provided the field and its gradient are known.

The ratio is expressed as follows using a different, dimensionally reduced form from ASTM F2052-15's Appendix X3:

$$\frac{\chi}{\rho\mu_0 g} = \frac{\tan \alpha}{B_0 \frac{dB_0}{dz}} \quad (2.7)$$

This formulation explains why the measured deflection angle  $\alpha$  (and thus  $F_m$ ) depends not on  $\chi$  or  $B_0$  independently, but on their product. Practically, this insight justifies our lab methodology: although our solenoid generates only 20 Gauss, we used a highly ferromagnetic sample (large  $\chi$ ), allowing us to replicate clinically relevant force-to-weight ratios ( $F_m/mg$ ).

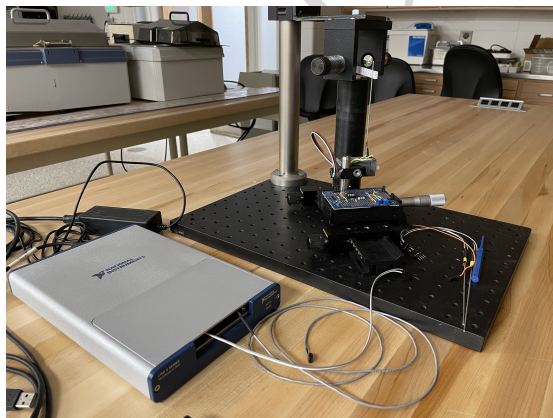
In the clinical MRI environment,  $B_0$  may reach 3 T, but the  $\chi$  of implanted materials is often orders of magnitude smaller. This inverse balance preserves the translational force regime, and supports translating results from lab simulations to clinical conditions.

All measurements were logged in **Microsoft Excel**, and photos/videos were captured via smartphone to document behavior. A minimum of **three trials** were performed for each current level; however, only the final (most consistent) dataset was retained for analysis. Data were exported to a Jupyter Notebook for clean up and processing with pandas. Then plotted to evaluate  $\tan \alpha$  vs. field gradient force. Propagated uncertainties in  $\alpha$  and  $dB_0/dz$  were computed using standard error propagation formulas.

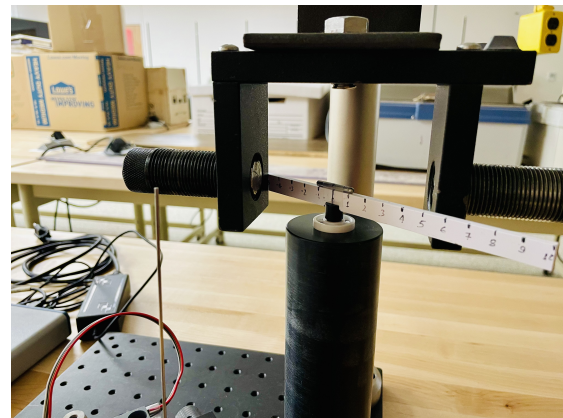
### In Clinic Measurement Protocol

#### 2.0.3 Torque Measurement Apparatus (In Progress)

A torque measurement system based on ASTM F2213 is under development. While a prototype was fabricated under the supervision of Dr. Nichols and prior students, detailed calibration, operational workflow, and data acquisition methods are still being finalized. The system is expected to allow both qualitative torque threshold assessments and quantitative torque calculation by assessing rotational displacement under a known static field. This device is shown in figure 2.8.



(a) Current torque measurement device



(b) Close up to the neodymium magnets and test sample (cylindrical metallic piece) were torques are applied.

Figure 2.8: Implementation of the apparatus in the laboratory setting.

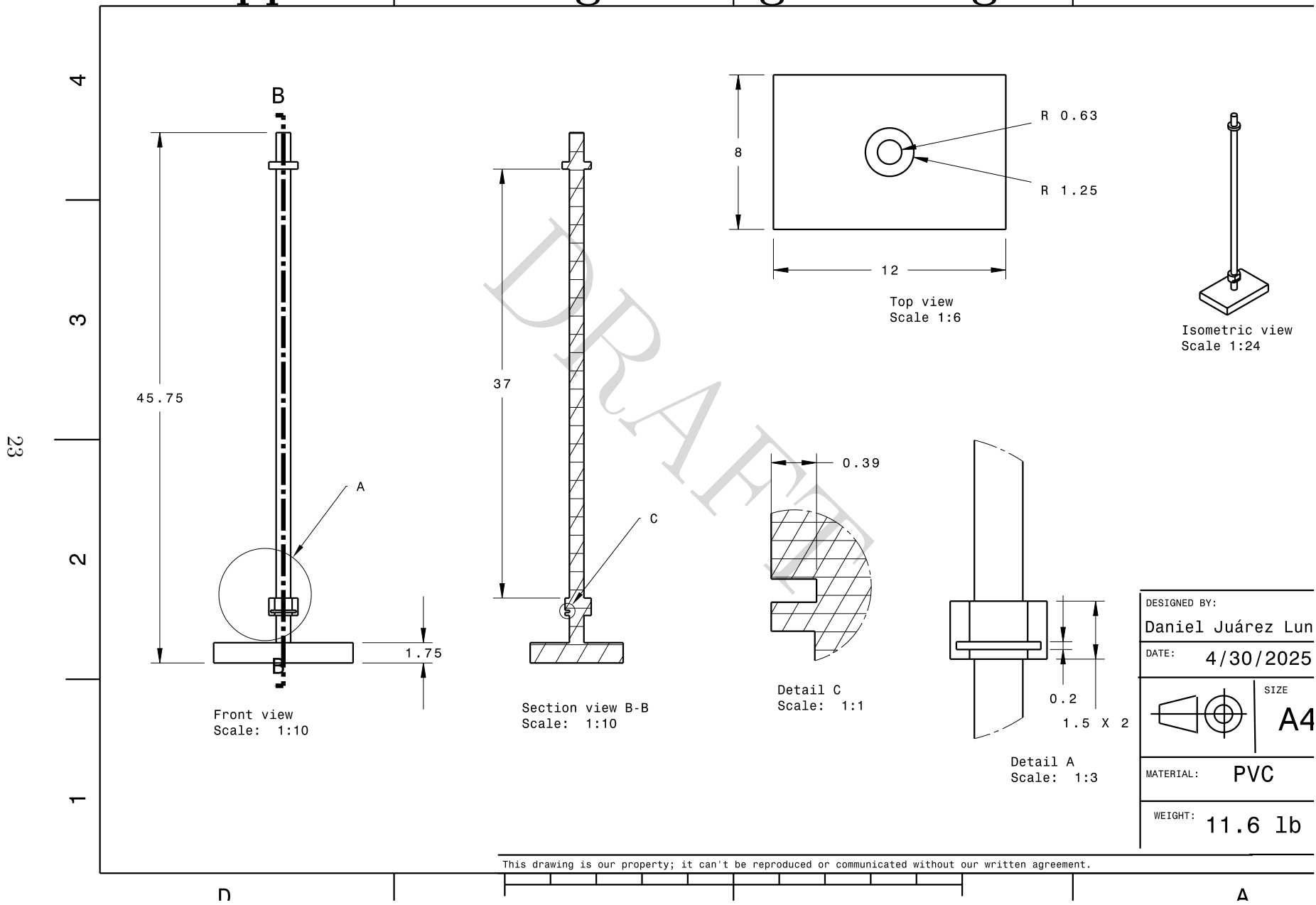
## **Appendix A**

### **Engineering Drawings**

DRAFT

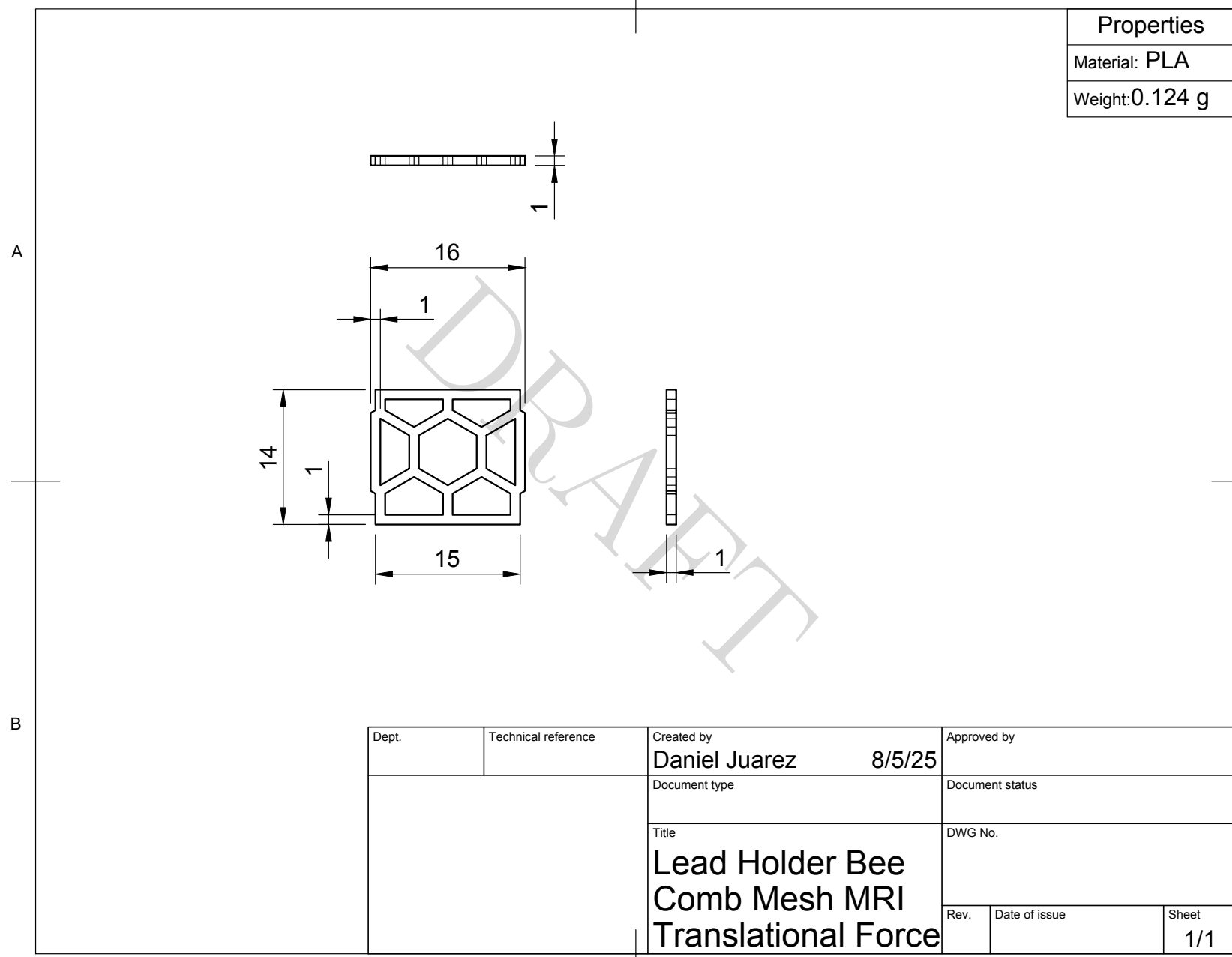
# Appendix A1: Pole drawing

## Appendix A: Engineering Drawings



## Appendix A2: Frame drawing

24



## Appendix B

### Calibrations

#### Appendix B: Calibration Logs and Supplementary Graphs

Additional experimental relationships and fitting diagnostics are presented to support the main analysis.

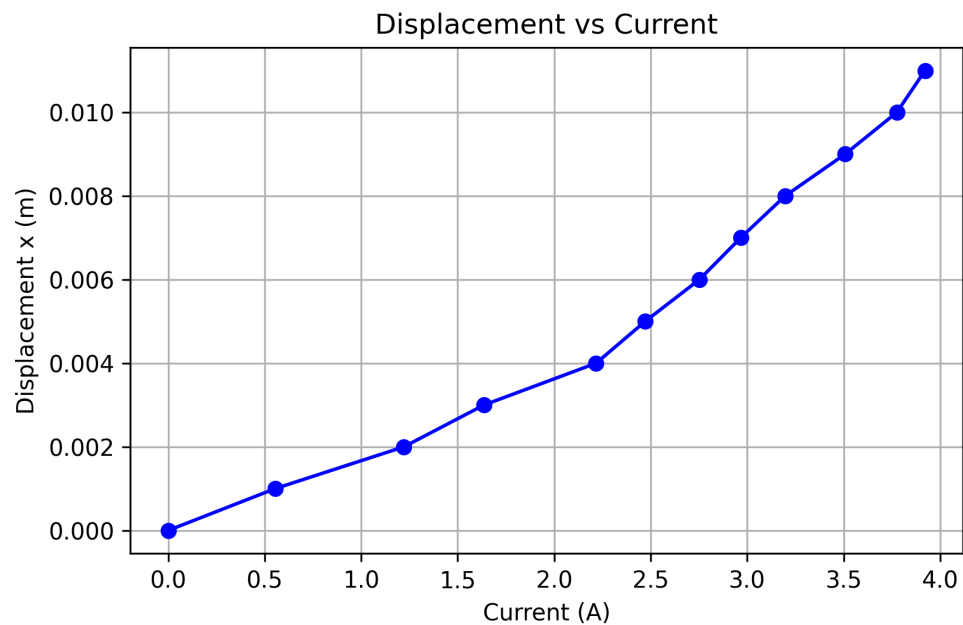


Figure B.1: Displacement as a function of current through the solenoid.

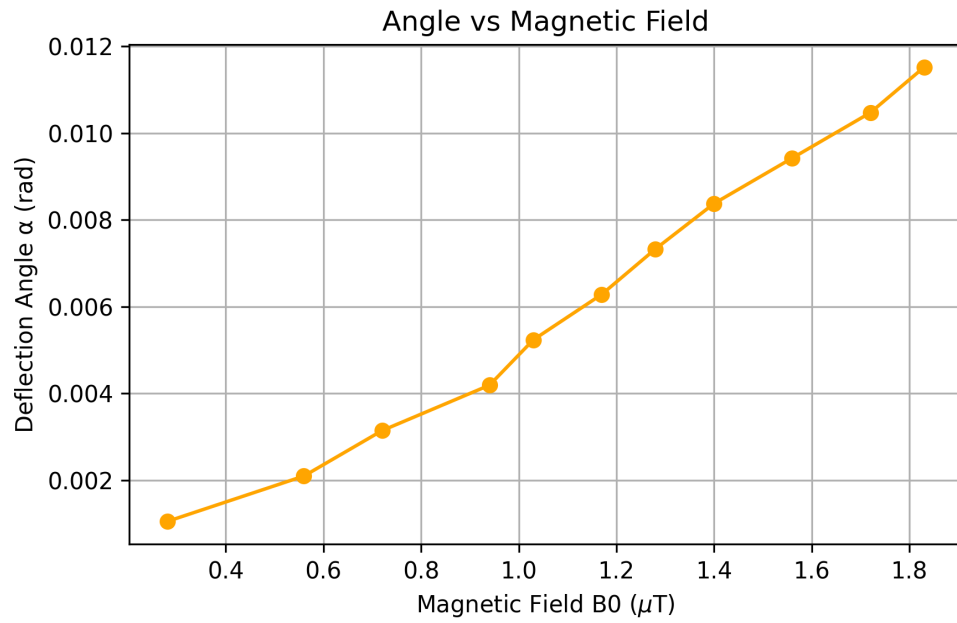


Figure B.2: Measured angle  $\alpha$  versus magnetic field intensity  $B_0$ .

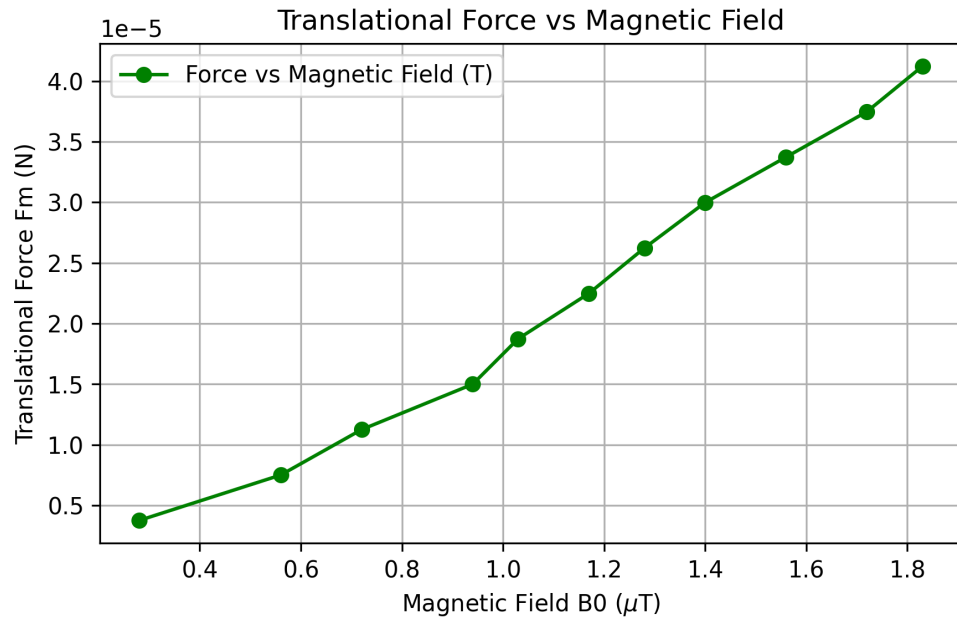


Figure B.3: Computed translational force  $F_m$  as a function of  $B_0$ .

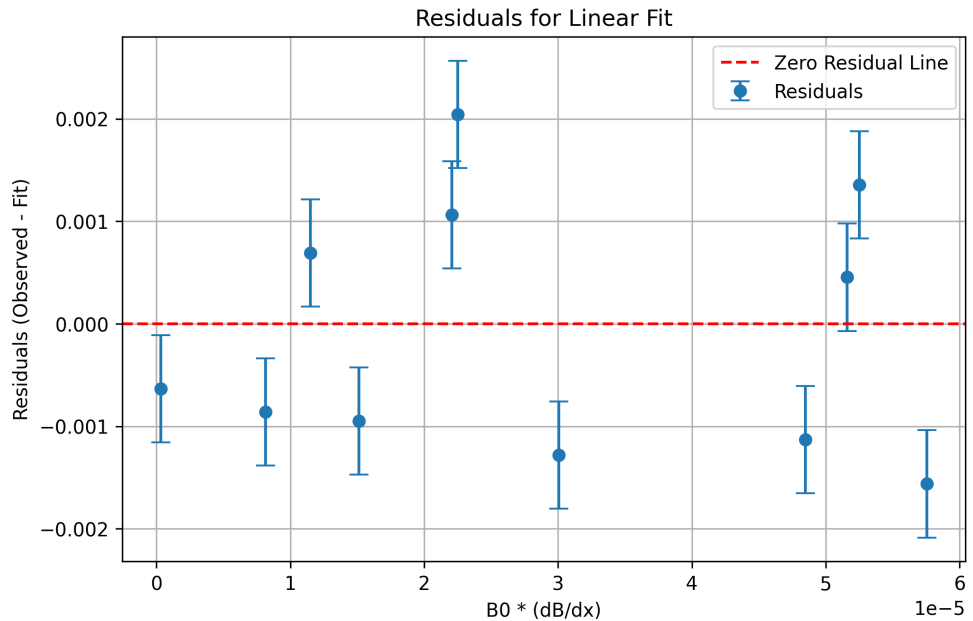


Figure B.4: Residuals from linear fit of  $\tan(\alpha)$  vs.  $B_0 \cdot \frac{dB_0}{dz}$ . Error bars indicate propagated uncertainties.

### Magnetic Field Analysis with Different Uncertainty Types

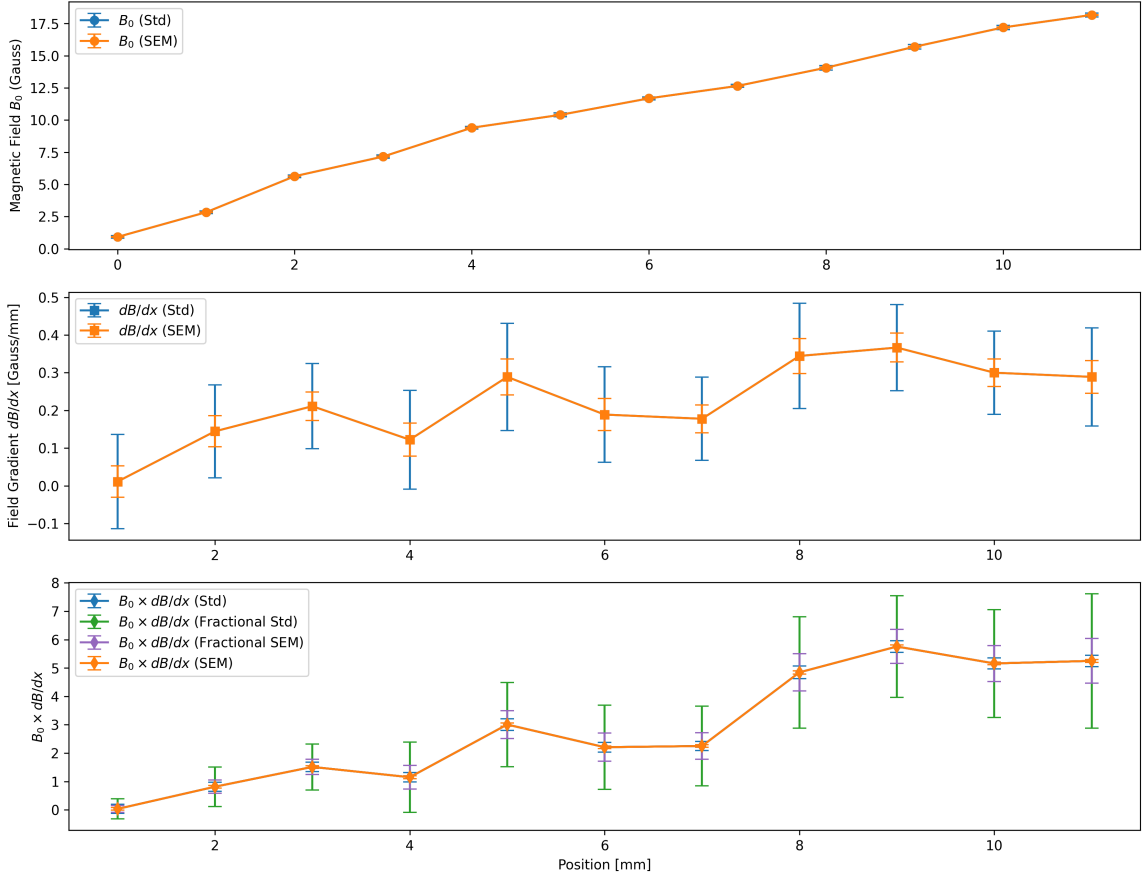


Figure B.5: Propagation of measurement uncertainty through magnetic field analysis. Top: Measured field  $B_0$  with standard deviation and SEM. Middle: Gradient  $dB/dz$  with propagated error. Bottom: Final product  $B_0 \cdot dB/dz$  with multiple uncertainty estimations (standard, fractional, SEM). This term was used as the independent variable in the susceptibility fit.

# Appendix C

## Copyright permissions

Unless you substantially alter a figure, you are not allowed to use figures from a published document, including journal articles, without copyright permission from the publisher. This is usually easily secured, without cost to you. Go to the journal article or book on the publisher's website, and find the Copyrights/Permissions link. Just fill out the form or follow instructions, and you will be emailed documentation of permission to use the figure in your thesis. For more information on using copyrighted figures in your thesis, see

<http://guides.lib.umich.edu/dissertationcopyright/otherscontent>.

You can include the copyright permissions in an appendix as figures or include a pdf using this command `\includepdf[scale=0.9]{rsna.pdf}`. If you do this, you could reference the appendix in each figure caption with “(See Appendix B for documentation of permission to republish from [cite source].)” Alternatively, you can save your permission documents into a separate document and include them as a separate upload to the Creighton Digital Repository (CDR). Make sure you note in your thesis that you are using the figure with permission. Please talk to Richard Jizba at the Creighton Library for advice.

# Glossary

**CDR** Creighton Digital Repository. 29

**CIED** cardiac implantable electronic device. 2

**ECG** electro cardigram. 1

**HRS** Heart Rhythm Society. 2

**MRI** Magnetic Resonance Imaging. vi, 1, 2, 3, 5, 11, 12, 17

**PD** Proton Density. 3

**PLA** Polylactic Acid. 15

**PVC** Polyvinyl Chloride. 11, 14

**RF** radiofrequency. 1, 2, 3, 5

**VI** LabVIEW Virtual Instrument (VI). 12

# References

- [1] T. Haddix. Creighton mri safety proposal (unpublished internal document), 2021. Creighton University.
- [2] A. Ferreira. Predicting angular displacement of medical devices in a mri scanner bore using comsol multiphysics. Master's thesis, Drexel University, 2017.
- [3] Heart Rhythm Society. Heart rhythm 2024 spotlights new developments in cardiac implantable electronic devices and other treatments. <https://www.hrsonline.org/news/hr24-spotlights-new-developments-cieds/>, May 2024. Accessed: 2025-07-07.
- [4] Fathima S Mubarak, Yevinka Ellepola, Kadijah Nyosha Chamba, Sanjay Agrawal, and Maged Makhoul. Complications of epicardial pacing wire removal following adult cardiac surgery: A systematic review. *Cureus*, 15(11):e49076, Nov 2023.
- [5] O. Aboyewa. *Measurement of Radiofrequency Induced Heating in Patients with Retained Post-Surgical Epicardial Leads During MRI*. PhD thesis, Creighton University, 2021.
- [6] G G Hartnell, L Spence, L A Hughes, M C Cohen, R Saouaf, and B Buff. Safety of mr imaging in patients who have retained metallic materials after cardiac surgery. *American Journal of Roentgenology*, 168(5):1157–1159, 1997. PMID: 9129404.

- [7] Pennsylvania Patient Safety Authority. Pennsylvania patient safety advisory—volume 3, issue 2 (june 2006): “mitigating look-alike/sound-alike medication errors”. [https://patientsafety.pa.gov/ADVISORIES/Pages/200603\\_08.aspx](https://patientsafety.pa.gov/ADVISORIES/Pages/200603_08.aspx), June 2006. Accessed: 2025-07-09.
- [8] M. C. Reade. Temporary epicardial pacing after cardiac surgery: a practical review. *Anaesthesia*, 62(4):364–373, 2007.
- [9] P. G. Poh, C. Liew, C. Yeo, L. R. Chong, A. Tan, and A. Poh. Cardiovascular implantable electronic devices: a review of the dangers and difficulties in mr scanning and attempts to improve safety. *Insights into Imaging*, 8(4):405–418, 2017.
- [10] Rahul G. Muthalaly, Nitesh Nerlekar, Yin Ge, Raymond Y. Kwong, and Arthur Nasis. Mri in patients with cardiac implantable electronic devices. *Radiology*, 289(2):281–292, 2018.
- [11] American College of Cardiology. Current State of MRI With Cardiac Devices. <https://www.acc.org/Latest-in-Cardiology/Articles/2024/05/21/10/30/Current-State-of-MRI-With-Cardiac-Devices>, May 2024. Expert Analysis, published May 21, 2024.
- [12] AM Vuorinen, R Paakkonen, J Karvonen, J Sinisalo, M Holmstrom, S Kivistö, J Peltonen, and T Kaasalainen. Mri safety with abandoned or functional epicardial pacing leads. *European Heart Journal - Cardiovascular Imaging*, 22(Supplement 2), 2021.
- [13] Claudia Meier, Carsten Israel, Michel Eisenblätter, Annika Hoyer, Ferdinand Valentin Stoye, Ali Yilmaz, and Stephan Gielen. Safety of magnetic resonance imaging in patients with cardiac implantable electronic devices and aban-

- doned or epicardial leads: A systematic review and meta-analysis. *Europace*, 26(6):euae165, 2024.
- [14] Jerrold T. Bushberg, J. Anthony Seibert, Edwin M. Leidholdt, and John M. Boone. *The Essential Physics of Medical Imaging*. Lippincott Williams & Wilkins, 3rd edition, 2011.
- [15] Lawrence P. Panych and Bruno Madore. The physics of mri safety. *Journal of Magnetic Resonance Imaging*, 47(1):28–43, 2018.
- [16] Dan Stoianovici, Karun Sharma, and Kevin Cleary. Measurement of magnetically induced torque on lightweight medical devices in the magnetic resonance environment for astm f2213. *IEEE Transactions on Biomedical Engineering*, 71(1):36–44, 2024.
- [17] Astm f2052-21 standard test method for measurement of magnetically induced displacement force on medical devices in the magnetic resonance environment, 2021. ASTM International.
- [18] Astm f2182-19 standard test method for measurement of radio frequency induced heating on or near passive implants during magnetic resonance, 2019. ASTM International.
- [19] AlphaLab Inc. Alphaapp. <https://www.alphalabinc.com/alphaapp/>, 2023. Software for data logging, streaming, and plotting; lacks adjustable sampling frequency control.
- [20] AlphaLab Inc. Alphalab data acquisition communication protocol. [https://www.alphalabinc.com/wp-content/uploads/2018/02/alphaapp\\_comm\\_protocol.pdf](https://www.alphalabinc.com/wp-content/uploads/2018/02/alphaapp_comm_protocol.pdf), 2018. Used to implement custom sampling control via LabVIEW VI.